Polymorphism and Interactions of a Viral Fusion Peptide in a Compressed Lipid Monolayer

Gerhard Schwarz and Susanne E. Taylor
Department of Biophysical Chemistry, Biocenter of the University, University of Basel, CH-4056 Basel, Switzerland

ABSTRACT With a view toward possible new insights into viral fusion mechanisms, we have investigated the HIV-1 gp41 fusion peptide in a monomolecular film of the biomembrane lipid palmitoyloleoylphosphatidylcholine. Its surface activity at an air/water interface was measured under equilibrium conditions, using the conventional Langmuir trough technique. Through a novel thermodynamic analysis, the partial molecular area of the peptide in the lipid moiety could be determined as a function of the lateral pressure and the interfacial peptide/lipid ratio. This indicates an orientation of the peptide backbone parallel to the lipid hydrocarbon tails. The molecular area decreases significantly upon monolayer compression, suggesting a conformational transition from a somewhat compact configuration to a more extended, presumably β-strand structure when a lipid packing density is approached that is generally believed to mimic the physical state of a biological membrane. Up to a lateral pressure of ~15 mN/m, practically all peptide inserts into the lipid monolayer. At higher compression a distinct partitioning into the aqueous subphase is observed. Under these conditions the data also reflect a strong aggregation of the lipid-associated peptide. Beyond a critical peptide/lipid ratio, the peptide's area requirement was found to become substantially enhanced, possibly because of the formation of water-filled pores.

INTRODUCTION

Entrance of an enveloped animal virus into a host cell is mediated by specific fusion proteins spanning the viral membrane (Marsh and Helenius, 1989). The molecular mechanism of such a process has so far not been satisfactorily elucidated (Stegmann, 1994). In particular, the issue of the possible formation of a proteinaceous pore in the target membrane has led to controversial discussions (Siegel, 1993; Colotto et al., 1996). Experimental evidence of relevant structures by means of patch-clamp studies was reported for the hemagglutinin of influenza virus (Spruce et al., 1989; Tse et al., 1993). More recently this has been confirmed by a fluorescence assay (Blumenthal et al., 1996). There is as yet no corresponding information on the human immunodeficiency virus (HIV). Nevertheless, the N-terminal sequence of 23 amino acid residues of the gp41 protein in the viral envelope has been identified as a putative fusion peptide (Gallaher, 1987). Synthesized samples of it are poorly soluble in water but exhibit a pronounced surface activity at the air/water interface (Rafalski et al., 1990). If bound, this peptide spans only half of a lipid bilayer (Brasseur et al., 1988; Gordon et al., 1992). Thus fundamental structural and thermodynamic data regarding the peptide's interaction with a lipid monolayer may be acquired with the conventional Langmuir trough technique.

This approach takes advantage of measurement of the surface pressure exerted on the barriers that confine a monomolecular film of amphiphilic material. The results may be analyzed in terms of the interfacial molecular areas and mutual energetic interactions. In recent decades special attention has been directed toward so-called insoluble monolayers (Gaines, 1966). These are presumed to lack any appreciable desorption into the aqueous subphase, so that the interfacial molecular area could be readily calculated from the trough area and the amount of added surfactant. Such a premise has been considered for biological lipids in particular. Their packing density at surface pressures around 30 mN/m concurs with that of a cell membrane (Marsh, 1996a). Accordingly, a compressed lipid monolayer can be regarded as a basic model for investigating the effect of biomembrane active agents, particularly peptides or proteins that are soluble to some extent in the aqueous environment.

Naturally, for a reliable quantitative analysis of relevant surface activity data, the actual partitioning of the added material between the interfacial and bulk volume phases must be known. Because in such a case only quantities on the order of nanomoles can be accommodated in the surface area of an ordinary Langmuir trough, even appreciable desorption gives rise to only nanomolarity concentrations in the subphase, which would easily escape direct detection. We have therefore endeavored to solve the problem by means of a novel procedure for collecting and evaluating data derived from measurements of surface pressure versus trough area. Our approach was first applied to the present fusion peptide on a clean air/water interface (Schwarz and Taylor, 1995). In these experiments with a single surfactant component, pressure/area isotherms had been recorded under equilibrium conditions for a number of different total amounts of the peptide. Because of the law of mass conservation, a plot of these amounts versus the respective film area at a given surface pressure results in a straight line

Received for publication 9 September 1998 and in final form 26 February 1999.

Address reprint requests to Dr. Gerhard Schwarz, Department of Biophysical Chemistry, Biocenter of the University, University of Basel, Klingelbergstrasse 70, CH 4056 Basel, Switzerland. Tel.: +41-61-267-2200; Fax: +41-61-267-2189; E-mail: schwarzg@ubaclu.unibas.ch.

0006-3495/99/06/3167/09 $2.00

whose slope is equal to the effective surface concentration, whereas the intercept on the ordinate reflects the amount being dissolved in the subphase. The method has been further applied to the same fusion peptide under a change of pH (Taylor and Schwarz, 1997), to the bee venom factor melittin (Wackerbauer et al., 1996), and to the lipid palmitoyloleoylphosphatidylcholine (POPC) (Schwarz et al., 1996).

When some peptide is added to a lipid film, a possible insertion is readily detected by the inherent increase in monolayer area at constant pressure. However, to calculate the area per inserted peptide molecule, its interfacial molar fraction must be determined. To this end we have extended our previous mass conservation approach to a mixture of two surfactant components. Preliminary accounts have been given elsewhere (Schwarz and Taylor, 1997a,b). Here we present an improved and more detailed analysis. It provides highly interesting quantitative information on structural and thermodynamic features of the viral fusion peptide under consideration upon its insertion into a membrane mimicking lipid film. Our approach is regarded as an alternative approach to the study of molecular properties of peptide-lipid interactions in addition to possible other methods, such as infrared spectroscopy by means of reflection-absorption at the air/water interface (Flach et al., 1996) or internal reflectance in supported monolayers (Axelsen et al., 1995).

THEORETICAL

The present line of conducting and exploiting experiments may be generally applied to any sparingly soluble two-component surfactant system. In particular, we consider a practically insoluble monolayer of a first surfactant to which another surfactant is added that can possibly partition between the interfacial and subphase domains. Mass conservation of the second surfactant accordingly implies

$$n_2^{\circ} = r \cdot n_1 + n_2^{s} \tag{1}$$

where n_2°, n_2^{s} stand for the total and subphase amounts, respectively; n_1 is the amount of the insoluble surfactant; and $r = n_2/n_1$ denotes the interfacial mixing ratio. To make full use of that rather trivial relation, we shall establish experimental conditions resulting in different pairs n_2°, n_1 but constant values of r and n_2^{s}. Then a plot of n_2° versus n_1 must be a straight line whose slope and ordinate intercept are equal to r and n_2^{s}, respectively. Provided that a partitioning equilibrium exists, the conditions to be observed are invariable values of both the surface pressure, π, and of $A^* = A/n_1$, which is the monolayer area (A) per amount of the first surfactant (i.e., the reciprocal of its surface concentration). This assertion can be rigorously deduced on the basis of thermodynamic principles, as will be briefly outlined in the following. For a more detailed argumentation, we refer to the Appendix.

A monomolecular film at the air/water interface defines a two-dimensional phase (σ). When kept at equilibrium, any of its thermodynamic properties will be a function of only four independent variables, which may, in addition to A, be chosen as the amounts of the three independent material components, i.e., n_o (interfacial water), n_1, and n_2, respectively. The variables T (temperature) and p (external pressure) are assumed to be constant and will therefore be ignored here. In particular, changes in the interfacial Gibbs free energy may thus be expressed in terms of its total differential:

$$dG_{\sigma} = \mu_o dn_o + \mu_1 dn_1 + \mu_2 dn_2 + \gamma dA \tag{2}$$

involving the respective interfacial chemical potentials μ_i ($i = 0, 1, 2$) and the surface tension γ.

If the interface has also established a thermodynamic equilibrium with its three-dimensional subphase (s), individual chemical potentials of the various components must have assumed the same values in both phases. Therefore, μ_o has to be equal to the chemical potential of the bulk aqueous solvent, which remains constant under our conditions (because the soluble surfactant is supposed to enter the subphase in only very small amounts). Taking into account the identity of second derivatives of G_{σ} irrespective of the order of differentiation, it follows from Eq. 2 that μ_1, μ_2 and $\pi = \gamma_o - \gamma$, respectively (where γ_o applies to the surfactant-free solvent) do not depend on n_o. Furthermore, we note that these intensive functions of state depend only on ratios of the remaining variables n_1, n_2, and A. Thus we can generally establish the functional relationship

$$\mu_1, \mu_2, \pi = f(r, A^*) \tag{3a}$$

or alternatively,

$$\mu_1, \mu_2, r = f(\pi, A^*) \tag{3b}$$

by virtue of exchanging independent variables (i.e., functional inversion). In other words, the chemical potentials as well as the interfacial mixing ratio are determined solely by π and A^*. The subphase concentration, c_2, another intensive variable of the system, is also subject to such a relationship. We can simply infer this from the condition of a partitioning equilibrium, namely,

$$\mu_2(\pi, A^*) = \mu_2^{\infty} + RT \cdot \ln c_2 \tag{4}$$

with μ_2^{∞} standing for the conventional standard chemical potential in the subphase (and taking c_2 to be small enough to ignore nonideal interactions). Invariable values of π and A^* must accordingly keep r and c_2 definitely fixed. A constant bulk volume, V, will then also fix n_2^{s} ($= V \cdot c_2$). This completes the conditions for a linear mass conservation plot according to Eq. 1.

By means of functional inversion, it is generally optional to choose, instead of π, A^*, any other appropriate pair of intensive parameters as independent variables that determine the overall thermodynamic state of the system. This conclusion remains uncontested, even if the given three independent components are involved in additional specific equilibria (leading to, e.g., structural or aggregational

changes). The respective mass action and conservation laws will always ensure that no further independent variables are needed.

In this context we introduce the partial molar areas as functions of π and r, namely,

$$A_i(\pi, r) = (\partial A/\partial n_i)_{n_j,\pi} \quad (j \neq i) \quad (i, j = 1 \text{ or } 2) \tag{5a}$$

(which may be promptly converted to the respective partial areas per molecule). A change in film area at constant π and fixed mixing ratio ($dA = A_1 dn_1 + A_2 dn_2$) can easily be integrated, resulting in the so-called "additivity rule":

$$A = n_1 \cdot A_1 + n_2 \cdot A_2 \tag{5b}$$

which is actually a rigorous relation based on first principles.

MATERIALS and METHODS

Substances

The peptide comprises the N-terminal 23-residue sequence of the gp41 fusion protein derived from the HIV-1 strain LAV_{1a}, namely AVGIGALFLGFLGAAGSTMGARS (Rafalski et al., 1990). It was self-synthesized, dissolved before use in dimethyl sulfoxide (DMSO) (from Fluka, Buchs, Switzerland), and quantified by frequently repeated amino acid analysis to specify the concentration of stock solutions as described in full detail previously (Schwarz and Taylor, 1995). There we also specified the McIlvain buffer used in this study. The lipid 1-palmitoyl-2-oleoyl-*sn*-glycero-3-phosphocholine (POPC), dissolved in $CHCl_3$, was obtained from Avanti Polar Lipids (Alabaster, AL) and diluted with more $CHCl_3$ (Merck, Darmstadt, Germany). Stock solutions have repeatedly been checked for their actual concentrations by means of phosphate analysis (Böttcher et al., 1961). We have so confirmed the lipid's area per molecule of 78 $Å^2$ at 25 mN/m, as determined previously (Schwarz et al., 1996). This value was used to calculate the lipid content in a given monolayer.

Instrumentation

The measurements have been carried out with a Langmuir round trough manufactured by Mayer Feintechnik (Göttingen, Germany) according to the method of Fromherz (1975). It consists of eight compartments, each with an interfacial area of 45 cm^2. We have combined three of them for our experiments. Two Teflon-made barriers in the center of the trough could be moved to close in the monolayer area at a speed of 5 cm^2/min (corresponding to 5–17 $Å^2$/min of mean peptide/lipid molecular area, depending on the amount of interfacial surfactant). The effective trough area was calculated geometrically and picked up by an electronic device (monofilmmeter), together with the respective surface pressure as measured by a Wilhelmy platelet (made of filter paper no. 1; Whatman International, Maidstone, England). Calibration of both parameters has always been performed before each measurement series. We note that the Wilhelmy plate of the film balance gives rise to a monolayer area increment that had so far been generally overlooked (Welzel et al., 1998). This effect can be corrected for by an effective surface increment (depending on the plate size) added to the geometrical trough area. It results in a minor parallel shift toward larger interfacial areas, as far as the mass conservation plots are concerned. Thus the molecular areas (derived from the slope) remain unaffected. Only the subphase desorption (derived from the ordinate intercept) may prove to be somewhat reduced. In the special case of POPC, a reevaluation of our previous data (Schwarz et al., 1996) revealed that this lipid actually forms a practically insoluble monolayer. In the present case we determined an effective surface area increment of 2.9 cm^2. Thus the molecular area of the pure liquid has been computed from this corrected film area, assuming an insoluble monolayer. The aqueous subphase (volume $V = 74$ ml, pH 7.4, ionic strength 60 mM, 23 ± 1°C) was continuously stirred. Further technical details are described in our preceding relevant publications, as cited in the Introduction.

Film preparation and data collection

Our approach requires a fairly large extent of surface activity data under reasonably stable equilibrium conditions, covering a wider range of spread lipid and peptide amounts. We found that this could be accomplished in the least time-consuming manner by recording pressure-area isotherms with lipid and then successively increasing peptide quantities.

The typical experiment was carried out in the following way. Spreading was always done over a maximum trough area (of 135 cm^2), so that there was no lateral pressure. Compression was only started after a sufficiently long waiting period (in the range of 0.5–3 h), to allow the system to completely stabilize (as monitored by the initial pressure changes in the course of time). Having reached the end point of compression (usually at 35 mN/m), the monolayer was expanded back to the original maximum area. After another sufficient waiting period, the next isotherm was recorded. With this basic routine a series of isotherms have been recorded, starting with a given amount of pure lipid, where subsequently more and more peptide was added. A second isotherm with the initial pure lipid normally turned out to deviate slightly from the first one. In that case, however, the third one did reproduce the preceding isotherm, so we accepted that one as stable. The isotherms with added peptide could always be reproduced the first time.

Stability

To verify that these isothermic data do correspond sufficiently well to a stable equilibrium of our monolayer/subphase system, we have compared them with the results of isochoric measurements. Using troughs of fixed area, we have spread known amounts of material and waited for a stationary state (taking usually 30–60 min). These tests resulted in practically the same data observed with the isothermic mode but required much more time to collect a sufficient number of data for the thermodynamic analysis. In addition, we also tried the isothermic mode with the peptide spread first. This reversal of the order of spreading made no significant difference regarding our data (see also Schwarz and Taylor, 1997b). Injection of the same small amounts of peptide into the subphase tended to give an extremely slow rate of pressure increase, as already observed in the case of pure melittin (Wackerbauer et al., 1996). We note that under these circumstances the kinetic driving force of partitioning into the lipid monolayer is virtually nil, because one starts with an extremely small concentration gradient at the interface.

Mass conservation

Possible adsorption of lipid and/or peptide at the walls of the trough can be ruled out. The material used by the manufacturer to avoid adhesion is a special kind of highly condensed ultrapure Teflon with a nonporous, smooth surface. Experiments involving different accessible wall areas have indeed not affected our data (Schwarz and Taylor, 1995).

To our knowledge, DMSO is the only practically useful solvent for the present peptide. To probe its quality to ensure proper spreading, we have carried out tests in which some pure liquid was also spread on a preformed monolayer (of pure or mixed surfactant). Then we measured another isotherm, following our standard routine. After desorption of the added DMSO into the aqueous subphase, we observed the same isotherm as before, indicating that this solvent does not drag along lipid or peptide into the bulk volume. We also refer to our results (see below), which show that at low pressures all of the spread peptide remains accumulated in the monolayer.

RESULTS

In the present experiments the lipid takes the role of an insoluble first surfactant, whereas the peptide is regarded as a poorly soluble second surfactant. For a given lateral pressure the increase in surface area, ΔA, under equilibrium conditions was determined from our various series of pressure versus trough area isotherms. Because we have to take into account here only differences in the area, the Wilhelmy plate effect cancels out, so it can be ignored.

For a given amount of lipid in the monolayer, n_L, we have plotted $\Delta A^* = \Delta A/n_L$ versus n_P°. Such experiments were primarily conducted with n_L/nmol = 6.22 and 13.35, respectively, comprising a broad range of added peptide amounts in two independent series of titrations each. Additional experiments with n_L/nmol = 4.76 and 9.25, respectively, have been run to confirm the quality of the linear mass conservation plots. At sufficiently low pressure, all ΔA^*-n_P° plots proved to be well-pronounced straight lines. Pertinent examples applying to $\pi = 10$ mN/m are presented in Fig. 1 *A*. The interpolated n_P° values for the individual n_L at the same level of ΔA^* must be subject to constancy regarding the interfacial peptide/lipid ("binding") ratio, $r = n_P/n_L$, and the amount that was partitioned into the subphase, n_P^s. Two special cases of the pertinent mass conservation plots according to Eq. 1 are shown in Fig. 1 *B*. They are indeed linear and do practically run through the origin (within a statistical measuring uncertainty of about ± 0.02 nmol), demonstrating virtually full insertion of the peptide into the lipid film.

For higher lateral pressures, actual partitioning into the bulk volume did definitely appear to a greater and greater extent. Concurrently, the ΔA^* versus n_P° curves become increasingly bent in the upward direction, as shown by the example for 25 mN/m exhibited in Fig. 2 *A*. The linear mass conservation plots in Fig. 2 *B* distinctly reveal a substantial portion of peptide that has entered the aqueous subphase.

This method of processing our data has been executed with pressures between 1 and 35 mN/m (mostly in steps of 1 mN/m). The range of practically complete "binding" of peptide by the lipid monolayer reached ~15 mN/m. Within that range the molecular area requirement of the peptide, a_P, can thus be simply derived from a plot of ΔA versus n_P°, as illustrated in Fig. 3. The observed linearity reflects a uniform value of a_P at a given lateral pressure below our upper limit of ~25% peptide per lipid.

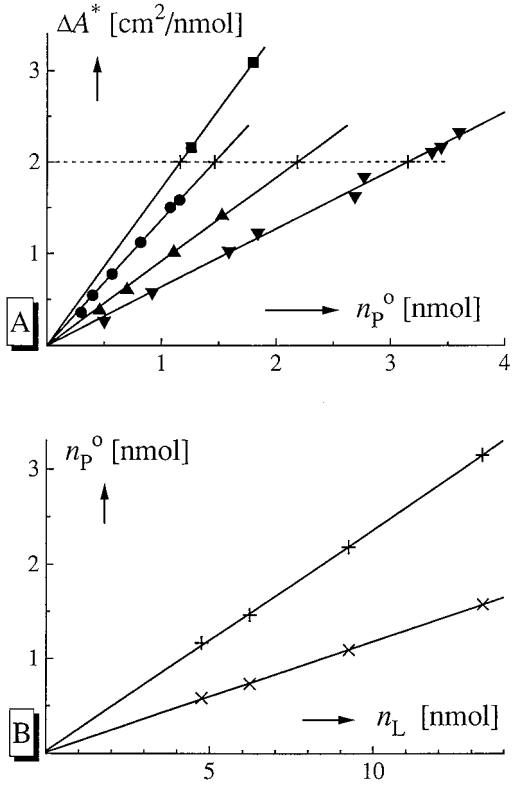

FIGURE 1 Data processing at 10 mN/m. (*A*) Plots of the measured area increase per lipid ($\Delta A^* = \Delta A/n_L$) versus total amount of added peptide, n_P°, for different amounts of lipid in the monolayer: n_L/nmol = 4.76 (■), 6.22 (●), 9.25 (▲), and 13.35 (▼). The crosses on the horizontal dashed line refer to n_P°, n_L pairs applying to the same surface and subphase concentrations (see text). (*B*) Mass conservation plots with n_P°, n_L pairs at constant ΔA^*/[cm²/nmol] = 2 (+) and 1 (×), respectively, taken from part *A*. The slopes reflect bound peptide/lipid ratios, $r = 0.234$ and 0.117, respectively, whereas the intercepts (n_P^s/nmol = 0.027 and 0.013) indicate practically negligible subphase concentrations.

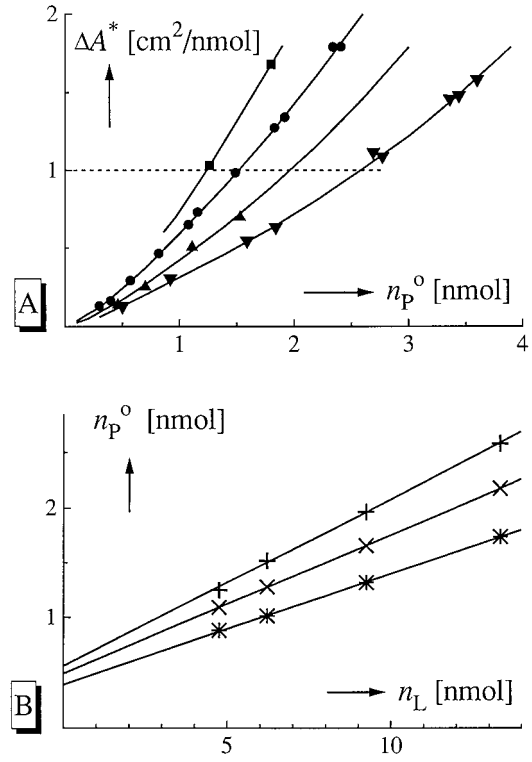

FIGURE 2 Data processing at 25 mN/m in analogy to Fig. 1. (*A*) The apparent upward curvature is due to aggregation of interfacially associated peptide (see text). (*B*) The linear mass conservation plots show pronounced intercepts on the ordinate axis, implying substantial amounts of peptide that have partitioned into the subphase. ΔA^*/[cm²/nmol] = 1.0 (+), 0.8 (×), and 0.6 (*), respectively.

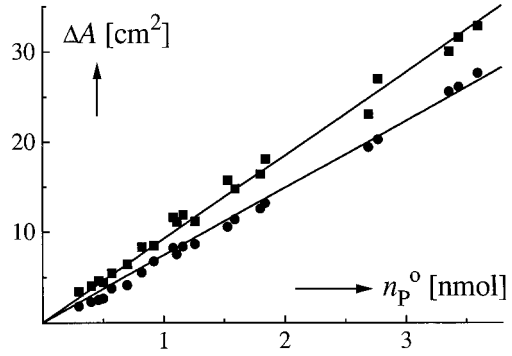

FIGURE 3 Plots of area increase upon the addition of a total amount of peptide, n_P°, for the examples of a lateral pressure π/[mN/m] = 5 (■) and 15 (●), respectively. The slopes result in A_P/[cm^2/nmol] = 9.25 (a_P = 154 Å^2) and 7.45 (a_P = 124 Å^2), respectively.

For a constant pressure we may now consider $A^* = A_L^\circ + \Delta A^*$ (A_L°: partial molar area of the pure lipid) as a function of the interfacial peptide/lipid ratio. Typical examples are displayed in Fig. 4. They can be examined in view of the relation

$$A^* = A_L + r \cdot A_P \tag{6}$$

which is readily established from Eq. 5b (A_L, A_P are the partial molar areas of the lipid and peptide, respectively.) We note that for $r \rightarrow 0$, the course of A^* can be linearly extrapolated toward A_L°. Nevertheless, the lipid packing density may change in the vicinity of inserted peptide. Because such a solvation effect should increase in proportion to r, these area changes would be included in the apparent value of A_P as derived from the slope of the A^*-r plots. Accordingly, the so determined molecular area, a_P (= A_P/N_A, N_A: Avogadro's number), will not necessarily reflect the true area requirement of the inserted peptide molecules. At any rate, our measured a_P undergoes quite suddenly a substantial change to a larger value once r exceeds a critical value r_c. This is clearly manifested by the sharp bend in the plots of A^* versus r. The magnitude of r_c decreases markedly upon compression of the monolayer, as shown by Fig. 5. Below ~16 mN/m it appears to fall above our measuring range of r. The low-r and high-r molecular areas, a_P and $a_P^\oplus$, respectively, as they depend on pressure, are presented in Fig. 6.

The partitioning equilibrium of peptide between the lipid and aqueous moieties is most conveniently described in terms of the fundamental relationship

$$r = f(\pi, c_P) \tag{7}$$

which is a possible alternative of Eq. 3b resulting from an exchange of the variable A^* with c_P (i.e., the subphase concentration of the peptide). Because here the bulk volume was held fixed, we prefer to plot r versus n_P^s, the amount of free peptide (note that an amount of 1 nanomole is equivalent to a subphase concentration of 13.5 nM). Examples of these "binding" isotherms are exhibited in Fig. 7 for a number of different lateral pressures.

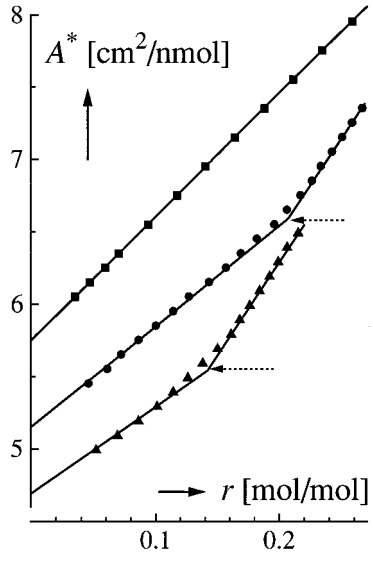

FIGURE 4 Monolayer area per lipid ($A^* = A/n_L$) plotted versus the interfacial peptide-to-lipid ratio at various fixed lateral pressures. These are π/[mN/m] = 10 (■), 18 (●), and 25 (▲). The slope of the curves is equal to the peptide's apparent partial molar area, A_P. Note the sharp bend at higher pressures, reflecting a substantially larger area requirement of the inserted peptide above a critical degree of incorporation, r_c (indicated by the *dashed arrows*).

DISCUSSION

We have presented a novel approach to processing surface activity data that is suited to determining separately the molecular area as well as the number of inserted and subphase dissolved molecules of a sparingly soluble surfactant added to an insoluble monomolecular film of another surfactant under equilibrium conditions. This is quite generally applicable to any such binary mixture in two dimensions, thus providing highly useful information about pertinent structural and thermodynamic features in quantitative terms. In particular, the method can be very well employed to

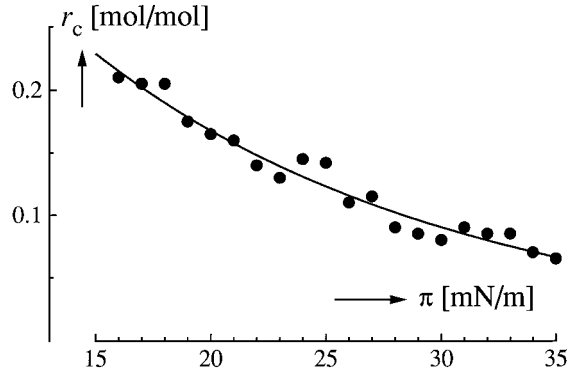

FIGURE 5 Pressure dependence of the critical peptide/lipid ratio, r_c, indicating a structural transition of inserted peptide aggregates toward a state of larger area requirement. The solid curve follows an exponential course.

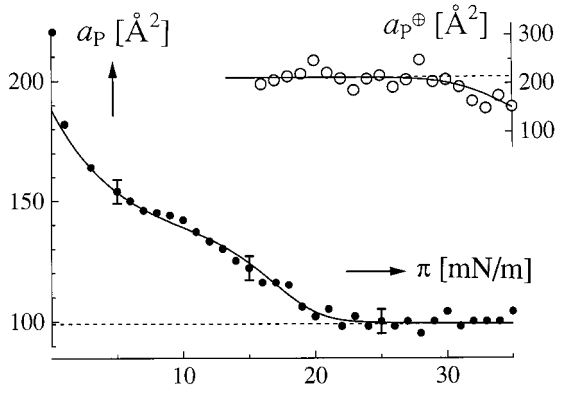

FIGURE 6 The peptide's molecular area as a function of the lateral compression. The solid points (●) refer to the values, a_P, applicable below r_c (the degree of uncertainty is about ±5 Å^2, as indicated). The open points (○) in the inset at the upper right represent $a_P^{\oplus}$, i.e., the considerably enhanced area requirements above r_c. The dashed line indicates a mean value of 215 Å^2 (standard deviation ±20 Å^2) in the range of 16–30 mN/m.

investigate the insertion of a peptide (or of any other membrane active agent) in a lipid monolayer, which is considered a basic model of a biomembrane. The present study demonstrates the potential of the proposed procedure in the special case of the putative HIV-1 gp41 fusion peptide acting on the lipid POPC.

This is, of course, an indirect method of getting access to the bulk concentration. A more direct measurement of those extremely small amounts of solute (in the nanomolar range) is, however, not feasible by standard techniques for a quantitative analysis. Even a radioactive tracer assay must be expected to suffer from a large error margin, as reported earlier in a monolayer study with a signal peptide (Tamm, 1986).

As far as the kinetics of peptide dissolution into the subphase is concerned, we would argue that a first step results in a transfer of peptide to an encounter layer just below the interfacial film. This may be subject to a rate-limiting activation energy barrier. A concentration gradient

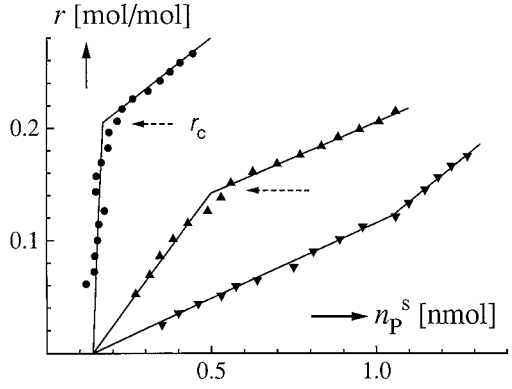

FIGURE 7 Examples of "binding" curves, i.e., plots of the peptide/lipid ratio in the monolayer versus the peptide amount in the subphase, n_P^s, for π/[mN/m] = 18 (●), 25 (▲), and 32 (▼). Note the apparent critical amount of peptide in the subphase at 0.14 nmol.

across the unstirred diffusion layer (which is generally considered to have a thickness of $\sim 10^{-3}$ cm) would then provide the driving force into the stirred bulk domain. That gradient will be much larger when the surfactant material is spread directly on the surface instead of being injected into the subphase. This would explain the fact that the latter mode of adding very small amounts of surfactant turns out to be very much slower in its progress toward equilibrium.

It must be emphasized that the present analysis of experimental data leads to an overall account of the amount of peptide as it partitions between the interface and the subphase. Accordingly, we can only calculate an average partial molecular area of the interfacial peptide, in case it exists in different structural states. In any event, this molecular area may also include a contribution from lipid density changes or from a possible pressure-induced curvature effect (Colotto et al., 1996).

Our mass conservation plots under a comparatively low lateral pressure up to ~15 mN/m (see Fig. 1 *B*) have shown that practically all of the spread peptide is incorporated into the lipid film. In such a case of full "binding" we have $r = n_P^{\circ}/n_L$, so that Eq. 6 predicts a straight line through the origin for the measured ΔA^* versus n_P° plots (at fixed n_L) as long as the apparent value of A_P does not change with increasing values of r. This is in accordance with our observations (see Fig. 1 *A*). The slope would simply be equal to A_P/n_L. After all, linearity should always occur in all such plots if a possible partitioning into the subphase can be described by a constant coefficient, k, in the relation $r = k \cdot n_P^s$, as it is applicable to a thermodynamically ideal partitioning process. Then the slope will be equal to $kA_P/(kn_L + 1)$. Its reciprocal value plotted versus n_L should result in a straight line whose slope and intercept give access to A_P and k.

However, when we turn to the situation in the higher compression range, our ΔA^* versus n_P° curves exhibit a pronounced upward bending (see Fig. 2 *A*). This can also explain the sigmoidal shape of the measured binding isotherms (see Fig. 7). There is an apparent critical value of n_P^s at ~0.14 nmol (c_P = 1.9 nM), which is a typical indication that large aggregates of solute are being formed in the lipid solvent. The apparently linear slope beyond that critical subphase content can be expressed as an ideal partitioning coefficient of those aggregates with the aqueous peptide moiety. Naturally that quantity will be reduced upon compression, because the chemical potential of monolayer-inserted peptide must increase at higher pressures.

Another sharp bend occurs in the "binding curves" at a critical peptide/lipid ratio, r_c (seen up to ~30 mN/m). At this same ratio, which decreases exponentially upon pressure (see Fig. 5), the A^*-r plots also exhibit a sharp bend, indicating a substantial increase in the peptide's apparent molecular area. This could very well reflect a structural transition of the aggregates that requires much more interfacial area.

Beyond ~30 mN/m the r_c bend can no longer be seen in the "binding" curves. Instead of this, an upward trend occurs above $r \approx 0.12$. This concurs with a slight drop in the

high molecular area requirement, possibly because of still another structural change in the lipid-inserted peptide aggregates. Altogether these features reflect a fairly complex case of molecular interactions and conversions that we cannot quantitatively analyze in greater detail at this time.

There are striking changes in the molecular area depending on compression. Interpretations in terms of structure may be attempted by sensible geometrical model calculations. The area requirement per molecule in the low-pressure range (≈200–130 Å^2) varies largely in proportion to the molecular area of the pure lipid. This may be attributed to the lateral compressibility experienced by a somewhat compact arrangement of the peptide when oriented parallel between the hydrocarbon chains of the lipid. An α-helix or an antiparallel β-hairpin seems to be a rather likely structure in view of the fact that their ideal cross-sectional areas fall in the proper range, as calculated from atomic structure data with a molecular modeling program (Taylor and Schwarz, 1997). In contrast to these findings, we had found without lipid but in the same pressure range a molecular area around 600 Å^2, indicating orientation parallel to a pure air/water interface (Schwarz and Taylor, 1995).

At higher compression, however, there is a clearly pronounced drop toward a quite smaller cross-sectional area. It suggests a conformation requiring only ~100 Å^2, presumably parallel β-strand configurations, which may be oriented slightly oblique in view of the ideal 80-Å^2 self-area in an orientation normal to the interface (Taylor and Schwarz, 1997). Polymorphism involving a coexistence of α-helical and β-strand structures in lipid bilayer membranes at comparable pH (but different experimental conditions) has indeed been reported in the literature (Gordon et al., 1992; Martin et al., 1993; Nieva et al., 1994; Pereira et al., 1997). In addition, an increasing peptide/lipid ratio was shown to induce an α-β conversion (Rafalski et al., 1990; Mobley et al., 1992; Martin et al., 1996). We also note that our interpretation of the observed molecular areas in the higher compression range is very consistent with some unpublished results obtained in another laboratory (Axelsen, personal communication). Using the technique of internal reflectance infrared spectroscopy (Axelsen et al., 1995) applied to the same peptide compressed at 20 mN/m in a supported lipid monolayer (90% POPC, 10% palmitoyloleoylphosphatidylserine (POPS)), the structure could be shown to be primarily β-sheet (with possibly some random and helical remains). An almost entirely β-sheet conformation was found for a slightly shortened 19mer peptide analog (in 100% POPC).

The rather dramatic increase in the apparent molecular area to some 215 Å^2 derived from the steeper slope in our A^* versus r plots beyond r_c (see Fig. 4) can hardly be explained by changes in the peptide's self-area alone. A hairpin-like antiparallel insertion would not allow intermolecular hydrogen bonding for aggregation. On the other hand, curvature effects as observed with bilayers (Colotto et al., 1996) would lead to an apparent decrease in area. We may conclude that the interfacial aggregates undergo a conversion into larger entities that somehow destabilize the lipid monolayer. This could be provoked by forming water-filled structural defects ("pores") in the lipid monolayer, possibly as β-barrels (Sansom and Kerr, 1995; Marsh, 1996b; 1997). Such an idea is in line with reports on destabilization and permeabilization of charged and uncharged lipid vesicle bilayers being caused by the same HIV-1 fusion peptide (Rafalski et al., 1990; Mobley et al., 1992; Pereira et al., 1995, 1997). The ratio, ρ, of pore area per monomer (including the aqueous lumen) over the peptide's actual molecular area may be calculated by means of a simple "barrel stave" model. With m cylindrical peptide monomers of cross-sectional radius $R_\bullet$ in the perimeter, one obtains

$$\rho = [\pi \cdot tg(\pi/m)]^{-1} + [1 + (2/m)]/2,$$

$$R_o = \{[\sin(\pi/m)]^{-1} - 1\} \cdot R_\bullet \qquad (8, 9)$$

where R_o is the inner pore radius. In our case of $\rho \approx 2$, this requires ~15 monomers for the average pore aggregate. With $R_\bullet \approx 5.6$ Å (for a self-area of 100 Å^2), we estimate an inner pore diameter of 4–5 nm. This agrees very well with the results of the already cited patch-clamp and fluorescence studies regarding the influenza virus case (Spruce et al., 1989; Tse et al., 1993). Its fusion peptide was also shown to induce area expansion and permeation when acting on lipid vesicles (Longo et al., 1997). For the latter virus it is actually known that several fusion proteins must interact in a fusion event, so that the formation of a pore involves larger aggregates of fusion peptide monomers (Ellens et al., 1990; Blumenthal et al., 1996). The virus can easily achieve this because the surface density of the fusion protein in the viral envelope is very high (Burger et al., 1991). Our present study suggests that the same holds true in the HIV-1 case.

Another possible explanation for the observed sudden increase in molecular peptide area could be a phase separation in the monolayer, resulting in lipid domains with some remaining peptide and pure peptide domains, in which the molecules tend to take on a more tilted orientation, as they do in a monolayer without lipid (Schwarz and Taylor, 1995). Whatever the underlying structural conversion is, it may play a significant role in the infection pathway of the AIDS virus. We expect that the existing alternatives can be narrowed down by supplementary work applying modern spectroscopic and/or microscopic techniques.

CONCLUSIONS

The molecular area and the insertion ratio of a strongly membrane active peptide in a lipid monolayer can be determined separately as a function of the lateral pressure by means of a novel approach utilizing conventional surface activity data under equilibrium conditions. This was demonstrated with the HIV-1 gp41 fusion peptide and the biomembrane lipid POPC.

In a lower compression range (below ~15 mN/m) the data reveal an apparent α-helical or β-hairpin conformation

of the peptide molecule, somehow oriented normal to the monolayer. Furthermore, practically no partitioning into the aqueous subphase takes place.

At higher compression (reaching into the lipid packing density of biomembranes) structural transitions toward more extended, presumably β-strand conformations are observed together with aggregation and appreciable subphase partitioning. Beyond a critical peptide/lipid ratio in the monolayer (that decreases upon compression), our results point to a structural transition of the peptide aggregates, possibly into water-filled pores or, alternatively, a peptide- and pressure-induced phase separation of the binary monolayer.

APPENDIX

Our theoretical foundation was only briefly presented in the main text. In view of its basic significance, a somewhat more detailed argumentation may be appropriate. We consider a system consisting of three independent material components whose total molar amounts are to be denoted n_i (i = 0, 1, 2). These components may interact with themselves and/or others to form all kinds of specific molecular structures, such as different conformations, aggregates, and complexes. A final equilibrium will nevertheless depend only on the given n_i and additional relevant variables of state (e.g., temperature, T, and external pressure, p). These variables do then control all thermodynamic properties of the whole system. In particular, this applies to the Gibbs free energy, G. Regarding any possible change of the equilibrium at constant T, p, where in addition to volume work some further reversible work dw has to be done, the change in G can generally be described by its total differential:

$$\mathrm{d}G = \mu_o \mathrm{d}n_o + \mu_1 \mathrm{d}n_1 + \mu_2 \mathrm{d}n_2 + \mathrm{d}w \qquad \text{(A1a)}$$

which defines the respective chemical potentials, μ_i, as the pertinent partial derivatives of G. When dealing with a closed system (allowing no exchange of material with the surroundings, so that $\mathrm{d}n_i = 0$) where dw is kept equal to zero, the condition of equilibrium will accordingly be

$$\mathrm{d}G = 0 \qquad \text{(A1b)}$$

indicating that G has reached a minimum under the circumstances.

In an interfacial monolayer (phase σ) we have $\mathrm{d}w = \gamma \mathrm{d}A$, so that the area, A, is to be introduced as an additional independent variable of state and the interfacial tension is $\gamma = \partial G/\partial A$. Because second partial derivatives must be equal independently of the order of differentiation, we have, for instance,

$$\partial \mu_1/\partial n_o = \partial \mu_o/\partial n_1 \qquad \text{(A2)}$$

Accordingly, it follows that μ_1 does not depend on n_o, provided that μ_o can be shown to be independent of n_1.

Turning now to a three-dimensional bulk solution (phase s) with a volume V, its change in G can be expressed analogously to Eq. A1a with $\mathrm{d}w = 0$ (assuming no reversible work is done in addition to volume work, $-p\mathrm{d}V$). The appropriate chemical potentials can be easily formulated according to convention when the solute amounts n_1, n_2 are extremely small in comparison with that of solvent, n_o. First of all, we have

$$\mu_o = \mu_o^* + RT \ln x_o = \mu_o^* - RT(x_1 + x_2) \qquad \text{(A3)}$$

where μ_o^* is the chemical potential of the pure solvent and the x are the respective molar fractions. Those of the solute would be on the order of 10^{-10} in our case (nanomole amounts of surfactant versus some 10 mol of water!). Their effect on μ_o can thus be absolutely neglected. In other words, we have in the subphase $\mu_o = \mu_o^*$, which naturally does not depend on the amounts of added surfactant. These components nevertheless have a chemical potential of their own, namely,

$$\mu_i = \mu_i^\infty + RT \ln c_i \quad (i = 1, 2) \qquad \text{(A4)}$$

where μ_i^∞ is the conventional standard potential at "infinite" dilution, and $c_i = n_i/V$ is the molar concentration.

In the event of a system that combines the interfacial monolayer and its subphase, the two individual dG according to Eq. A1a must be taken together. If there is only an exchange of material between the two phases and A is held constant, this leads to

$$\mathrm{d}G = \mathrm{d}G_\sigma + \mathrm{d}G_S = \sum_i (\mu_i^{(\sigma)} - \mu_i^{(s)}) \mathrm{d}n_i^{(\sigma)} = 0 \qquad \text{(A5)}$$

which takes into account $\mathrm{d}n_i^{(s)} = -\mathrm{d}n_i^{(\sigma)}$ (because of mass conservation) and the condition of an equilibrium in the whole system according to Eq. A1b. Therefore the chemical potentials of its individual components must have assumed equal values everywhere.

In particular, $\mu_o^{(\sigma)}$ (applying to interfacial water) will be fixed to μ_o^*. By virtue of Eq. A2 we conclude that μ_1 as well as (analogously) μ_2 and γ do only depend on n_1, n_2, and A. Because μ and γ (or, optionally, π) are intensive functions of state, they must remain invariant if each of those extensive variables is multiplied by the same factor (e.g., $1/n_1$). This implies that only their ratios are relevant independent variables, for instance, $r = n_2/n_1$ and $A^* = A/n_1$. Generally it follows from such reasoning that any intensive function of the whole system can be established as a function of these two variables. They may be exchanged, however, with another possible choice through functional inversion, e.g., with π, A^* or π, c_2.

Possible internal equilibria never lead to more independent variables. As an example, let us assume that surfactant 2 occurs in two different states, a and b. According to the equilibrium condition and mass conservation, we then have the two equations

$$\mu_a(r_a, r_b, \pi) = \mu_b(r_a, r_b, \pi); \quad r = r_a + r_b \qquad \text{(A6a,b)}$$

which can be used to express r_a and r_b as a function of r, π. By an analogous combination of pertinent mass action and mass balance laws, one can always reduce a possible multitude of specific concentration variables to the given minimum set provided by the total amounts of independent components.

We gratefully appreciate personal communications with Dr. Paul H. Axelsen (Department of Pharmacology, University of Pennsylvania), who made available to us his unpublished spectroscopic results. Furthermore, we thank Dr. Ingrid Weis for her help in some of the monolayer experiments and Christoph Stürzinger for his competent technical assistance (in performing phosphate analysis of the lipid).

This work has been supported by grants 21.45433.95 and 31.42045.94 from the Swiss National Science Foundation.

REFERENCES

Axelsen, P. H., W. D. Braddock, H. L. Brockman, C. M. Jones, R. A. Dluhy, B. K. Kaufman, and F. J. Puga, II. 1995. Use of internal reflectance infrared spectroscopy for the in situ study of supported lipid monolayers. *Appl. Spectrosc.* 49:526–531.

Blumenthal, R., D. P. Sarkar, S. Durell, D. E. Howard, and S. J. Morris. 1996. Dilation of the influenza hemagglutinin fusion pore revealed by the kinetics of individual cell-cell fusion events. *J. Cell Biol.* 135:63–71.

Böttcher, C. J. F., C. M. VanGent, and C. Pries. 1961. A rapid and sensitive sub-micro phosphorus determination. *Anal. Chim. Acta.* 24:203–204.

Brasseur, R., B. Cornet, A. Burny, M. Vandenbanden, and J.-M. Ruysschaert. 1988. Mode of insertion into a lipid membrane of the N-terminal HIV gp41 peptide segment. *AIDS Res. Hum. Retroviruses.* 4:83–90.

Burger, K. N., S. A. Wharton, R. A. Demel, and A. J. Verkleij. 1991. The interaction of synthetic analogs of the N-terminal fusion sequence of

influenza virus with a lipid monolayer. Comparison of fusion-active and fusion-defective analogs. *Biochim. Biophys. Acta.* 1065:121–129.

Colotto, A., I. Martin, J.-M. Ruysschaert, A. Sen, S. W. Hui, and R. M. Epand. 1996. Structural study of the interaction between SIV fusion peptide and model membranes. *Biochemistry.* 35:980–989.

Ellens, H., J. Bentz, D. Mason, F. Zhang, and J. M. White. 1990. Fusion of influenza hemagglutinin-expressing fibroblasts with glycophorin-bearing liposomes: role of hemagglutinin surface density. *Biochemistry.* 29:9697–9707.

Flach, C. R., F. G. Prendergast, and R. Mendelsohn. 1996. Infrared reflection-absorption of melittin interaction with phospholipid monolayers at the air/water interface. *Biophys. J.* 70:539–546.

Fromherz, P. 1975. Instrumentation for handling monomolecular films at an air-water interface. *Rev. Sci. Instrum.* 46:1380–1385.

Gaines, G. L. 1966. Insoluble Monolayers at Liquid-Gas Interfaces. Interscience Publishers, Wiley and Sons, New York.

Gallaher, W. R. 1987. Detection of a fusion peptide sequence in the transmembrane protein of human immunodeficiency virus. *Cell.* 50: 327–328.

Gordon, L. M., C. C. Curtain, Y. C. Zhong, A. Kirkpatrick, P. W. Mobley, and A. J. Waring. 1992. The amino-terminal peptide of HIV-1 glycoprotein 41 interacts with human erythrocyte membranes: peptide conformation, orientation and aggregation. *Biochim. Biophys. Acta.* 1139: 257–274.

Longo, M. L., A. J. Waring, and D. A. Hammer. 1997. Interaction of the hemagglutinin fusion peptide with lipid bilayers: area expansion and permeation. *Biophys. J.* 73:1430–1439.

Marsh, D. 1996a. Lateral pressure in membranes. *Biochim. Biophys. Acta.* 1286:183–223.

Marsh, D. 1996b. Peptide models for membrane channels. *Biochem. J.* 315:345–361.

Marsh, D. 1997. Stoichiometry of lipid-protein interaction and integral membrane protein structure. *Eur. Biophys. J.* 26:203–208.

Marsh, M., and A. Helenius. 1989. Virus entry into animal cells. *Adv. Virus Res.* 36:107–151.

Martin, I., F. Defrise-Quertain, E. Decroly, M. Vandenbanden, R. Brasseur, and J.-M. Ruysschaert. 1993. Orientation and structure of the NH_2-terminal HIV-1 gp41 peptide in fused and aggregated liposomes. *Biochim. Biophys. Acta.* 1145:124–133.

Martin, I., H. Schaal, A. Scheid, and J.-M. Ruysschaert. 1996. Lipid membrane fusion induced by the human immunodeficiency virus type 1 gp41 N-terminal extremity is determined by its orientation in the lipid bilayer. *J. Virol.* 70:298–304.

Mobley, P. W., C. C. Curtain, A. Kirkpatrick, A. J. Waring, and L. M. Gordon. 1992. The amino-terminal peptide of HIV-1 glycoprotein 41 lyses human erythrocytes and $CD4^+$ lymphocytes. *Biochim. Biophys. Acta.* 1139:251–256.

Nieva, J. L., S. Nir, A. Muga, F. M. Goñi, and J. Wilschut. 1994. Interaction of the HIV-1 fusion peptide with phospholipid vesicles. Different structural requirements for fusion and leakage. *Biochemistry.* 33:3201–3209.

Pereira, F. B., F. M. Goñi, A. Muga, and J. L. Nieva. 1997. Permeabilization and fusion of uncharged lipid vesicles induced by the HIV-1 fusion peptide adopting an extended conformation: dose and sequence effects. *Biophys. J.* 73:1977–1986.

Pereira, F. B., F. M. Goñi, and J. L. Nieva. 1995. Liposome destabilization induced by the HIV-1 fusion peptide. Effect of a single amino acid substitution. *FEBS Lett.* 362:243–246.

Rafalski, M., J. D. Lear, and W. F. DeGrado. 1990. Phospholipid interactions of synthetic peptides representing the N-terminus of HIV gp41. *Biochemistry.* 29:7917–7922.

Sansom, M. S. P., and I. D. Kerr. 1995. Transbilayer pores formed by β-barrels: molecular modeling of pore structures and properties. *Biophys. J.* 69:1334–1343.

Schwarz, G., and S. E. Taylor. 1995. Thermodynamic analysis of the surface activity exhibited by a largely hydrophobic peptide. *Langmuir.* 11:4341–4346.

Schwarz, G., and S. E. Taylor. 1997a. Peptide-lipid interactions in Langmuir monolayers. A novel approach toward structural and thermodynamic analyses. *Biophys. J.* 72:A120.

Schwarz, G., and S. E. Taylor. 1997b. Peptide-lipid interactions in Langmuir monolayers at the air/water interface. A novel thermodynamic analysis of a two-component surfactant system. *Supramol. Sci.* 4:479–483.

Schwarz, G., G. Wackerbauer, and S. E. Taylor. 1996. Partitioning of a nearly insoluble lipid monolayer into its aqueous subphase. *Colloids Surfaces A.* 111:39–47.

Siegel, D. P. 1993. Modeling protein-induced fusion mechanisms: insights from the relative stability of lipidic structures. *In* Viral Fusion Mechanisms. J. Bentz, editor. CRC Press, Boca Raton, FL. 475–512.

Spruce, A. E., A. Iwata, J. M. White, and W. Almers. 1989. Patch clamp studies of single cell-fusion events mediated by a viral fusion protein. *Nature.* 342:555–558.

Stegmann, T. 1994. Anchors aweigh. A recent study using a version of the influenza virus hemagglutinin protein in which its membrane anchor was replaced by a lipid tail provides new insights into how proteins can mediate the fusion of membranes. *Curr. Biol.* 4:551–554.

Tamm, L. K. 1986. Incorporation of a synthetic mitochondrial signal peptide into charged and uncharged phospholipid monolayers. *Biochemistry.* 25:7470–7476.

Taylor, S. E., and G. Schwarz. 1997. The molecular area characteristics of the HIV-1 gp41-fusion peptide at the air/water interface. Effect of pH. *Biochim. Biophys. Acta.* 1362:257–264.

Tse, F. W., A. Iwata, and W. Almers. 1993. Membrane flux through the pore formed by a fusiogenic viral envelope protein during cell fusion. *J. Cell Biol.* 121:543–552.

Wackerbauer, G., I. Weis, and G. Schwarz. 1996. Preferential partitioning of melittin into the air/water interface: structural and thermodynamic implications. *Biophys. J.* 71:1422–1427.

Welzel, P. B., I. Weis, and G. Schwarz. 1998. Sources of error in Langmuir trough measurements: Wilhelmy plate effects and surface curvature. *Colloids Surfaces A.* 144:229–234.